Dedicated to Academician Aureliu Sandulescu's 80^{th} Anniversary

DECAY THEORY BEYOND THE GAMOW PICTURE

D. S. DELION

Horia Hulubei National Institute for Physics and Nuclear Engineering,
P.O. Box MG-6, Bucharest, Romania
E-mail: delion@theory.nipne.ro

Received September 30, 2011

In the cluster emission theory the decay width is a product between the penetrability and reduced width. The first component gives the so-called "Gamow description" of the decay process, leading to the Geiger-Nuttall law. The second component is connected to clustering features and satisfies an analytic universal law, which is the next step beyond the standard Gamow rule. As a consequence, the reduced width can be described microscopically by using a mixed single particle basis with two components. The first part describes the usual spectroscopic properties, while the second one is connected to clustering features. The universal law implies that the harmonic oscillator parameter of the cluster part is proportional to the Coulomb parameter.

Key words: α-decay, cluster decay, proton emission, penetrability, reduced width.

PACS: 21.60.Gx, 23.60.+e, 23.70.+j.

1. INTRODUCTION

In the oldest Gamow approach of the α-decay process the α-particle was considered a preformed cluster, moving around the core and penetrating quantum mechanically the Coulomb barrier [1]. This may justify the so-called extreme cluster models, where the decay process is described by the penetration of the α-core Coulomb potential [2–4]. We will show that this picture is able to provide more informations, namely to provide a simple analytical relation, connecting the reduced width to the fragmentation potential. It is valid for any kind of decay process induced by the strong interaction, except fission, and it is the next natural step beyond the Gamow picture.

This phenomenological law has a direct consequence on the microscopic decay theory. The shell model provides the theoretical tool to compute microscopically the reduced width, proportional to the α-cluster amplitude inside the parent wave function [5, 6]. First calculations evidenced that the absolute decay widths were much smaller than the experimental values. In the late 1970's it was shown that the inclusion of many configurations is able to increase the value of the absolute decay width by more than four orders of magnitude [7]. This was not enough and only a theory where a combined shell- and cluster-model configurations were considered could reproduce the absolute decay width [8, 9]. We will show that this mixed representation is able to simultaneously describe α decay widths and electromagnetic transitions.

2. ANALYTIC RELATION FOR THE REDUCED WIDTH

For spherical emitters the decay width of the process $P(arent) \to D(aughter) + C(luster)$ is defined in terms of the scattering amplitude N_0 as follows [10]

$$\Gamma = \hbar v |N_0|^2 = \hbar v \left| \frac{R f_0^{(int)}(R)}{G_0(R)} \right|^2 , \tag{1}$$

where v is the velocity of the cluster-daughter system at infinity and $G_0(R)$ is the monopole irregular Coulomb function.

The above ratio does not depend on the cluster-daughter radius R, because both internal $f_0^{(int)}(R)$ and external $G_0(R)/R$ wave functions should satisfy the same Schrödinger equation. Traditionally the decay width is rewritten

$$\Gamma = 2 P_0 \gamma^2, \tag{2}$$

in terms of the penetrability and reduced width squared

$$P_0 = \frac{\kappa R}{|G_0(R)|^2}, \qquad \gamma^2 = \frac{\hbar^2}{2\mu R} |f_0^{(int)}(R)|^2, \tag{3}$$

where κ is the momentum and μ the reduced cluster-daughter mass.

The decay processes can be schematically described by the following cluster-daughter pocket-like spherical potential [10]

$$\begin{aligned} V(r) &= \hbar\omega \frac{\beta (R - R_0)^2}{2} + v_0, \quad R \le R_B \\ &= \frac{Z_D Z_C e^2}{R} \equiv V_C(R), \quad R > R_B \end{aligned} \tag{4}$$

where R_0 is the surface pocket radius. Notice that the radial equation of the shifted harmonic oscillator (ho) potential is similar with the equation of the one-dimensional oscillator. By considering Q-value as the first eigenstate in the shifted ho well $Q - v_0 = \frac{1}{2}\hbar\omega$, together with the continuity condition at the top of the barrier R_B, one obtains the following relation

$$\hbar\omega \frac{\beta (R_B - R_0)^2}{2} = V_{frag}(R_B) + \frac{1}{2}\hbar\omega, \tag{5}$$

where it was introduced the so called fragmentation (or driving) potential, as the difference between the top of the Coulomb barrier and Q-value

$$V_{frag}(R_B) = V_C(R_B) - Q = Q \left[\frac{\chi}{\rho} - 1 \right], \tag{6}$$

in terms of the Coulomb parameter and reduced radius, respectively

$$\chi = \frac{2 Z_D Z_C}{\hbar v} , \quad \rho = \kappa R. \tag{7}$$

For a shifted ho well one has for the ground state

$$|f_0^{(int)}(R)|^2 = A_0^2 e^{-\beta(R-R_0)^2}. \tag{8}$$

By using (5), one obtains the following relation

$$\log_{10}\gamma^2(R_B) = -\frac{log_{10}e^2}{\hbar\omega}V_{frag}(R_B) + \log_{10}\frac{\hbar^2 A_0^2}{2e\mu R_B}. \tag{9}$$

Notice that the slope in (9) has a negative value and it is connected with the shape of

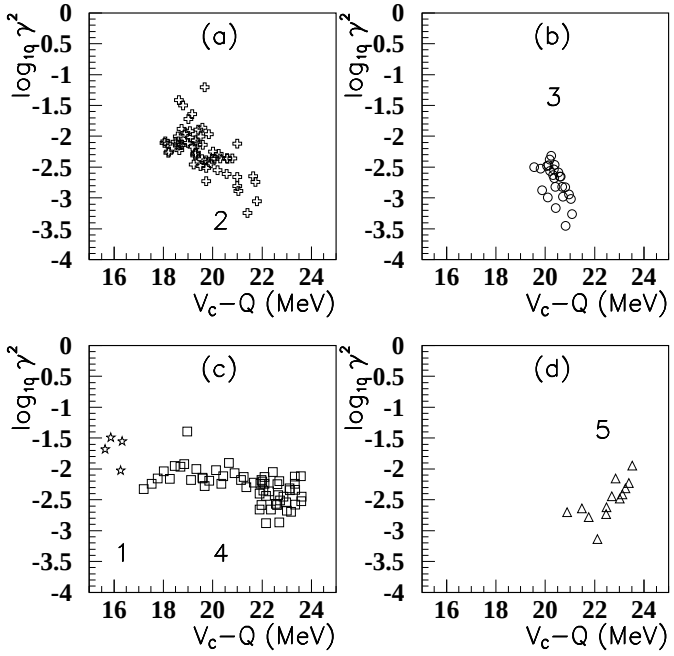

Fig. 1 – The logarithm of the α-decay reduced width squared versus the fragmentation potential (6) for regions of the nuclear chart described by (10).

the interaction potential (ho energy $\hbar\omega$), while the free term gives information about the amplitude of the cluster wave function. Our calculation has shown that the linear relation (9) but with different coefficients, remains valid in the most general case of the double folding plus repulsive interaction between fragments, used in [11, 12].

Most of experimental data refer to the α-decay. Therefore we analyzed (9) in α-decays connecting ground states of even-even nuclei. In figure 1 the data are

divided into five regions of even-even α emitters as follows

$$\begin{array}{lllll} 1) & Z<82, & 50<N<82 & \text{Fig. 1 (c), stars ;} \\ 2) & Z<82, & 82<N<126 & \text{Fig. 1 (a), crosses ;} \\ 3) & Z>82, & 82<N<126 & \text{Fig. 1 (b), circles ;} \\ 4) & Z>82, & 126<N<152 & \text{Fig. 1 (c), squares ;} \\ 5) & Z>82, & N>152 & \text{Fig. 1 (d), triangles .} \end{array} \tag{10}$$

In calculations it was used the value of the touching radius, *i.e.*

$$R_B = 1.2(A_D^{1/3} + A_C^{1/3}). \tag{11}$$

Notice that the regions 1-4 contain rather long isotopic chains, while in the last region 5 one has not more than two isotopes/chain. This is the reason why, except for the last region 5, the reduced width decreases with respect to the fragmentation potential, according to the theoretical prediction given by (9).

The linear dependence of $log_{10}\gamma^2$ versus the fragmentation potential (9) remains valid for any kind of cluster emission. This fact is nicely confirmed by heavy cluster emission processes in figure 2 (a). Here it is also plotted a similar dependence for α-decays corresponding to the same heavy cluster emitters. The straight line is the linear fit for cluster emission processes, except α-decays

$$log_{10}\gamma^2 = -0.586(V_C - Q) + 15.399. \tag{12}$$

The above value of the slope $-log_{10}e^2/\hbar\omega$ in (9) leads to $\hbar\omega \approx 1.5$ MeV, with the same order of magnitude as in the α-decay case.

Let us mention that a relation expressing the spectroscopic factor (proportional with the reduced width) for cluster emission processes was derived in [13]

$$S = S_\alpha^{(A_C-1)/3}, \tag{13}$$

where A_C is the mass of the emitted cluster and $S_\alpha \sim 10^{-2}$. As can be seen from figure 2 (b) between A_C and V_{frag} there exists a linear dependence and therefore the above scaling law can be easily understood in terms of the fragmentation potential.

Concerning the reduced widths of proton emitters in [14, 15] it was pointed out the correlation between the reduced width and the quadrupole deformation. This fact can be seen in figure 3 (a), where the region with $Z < 68$ corresponds to $\beta > 0.1$ (open circles), while the other one with $Z > 68$ to $\beta < 0.1$ (dark circles). The two linear fits have obviously different slopes. Notice that the two dark circles with the smallest reduced widths correspond to the heaviest emitters with $Z > 80$.

At the same time one sees from figure 3 (b) that the same data are clustered into two regions, which can be directly related with the fragmentation potential (6). Here, the two linear fits in terms of the fragmentation potential, corresponding to the two regions of charge numbers, have roughly the same slopes, but different values

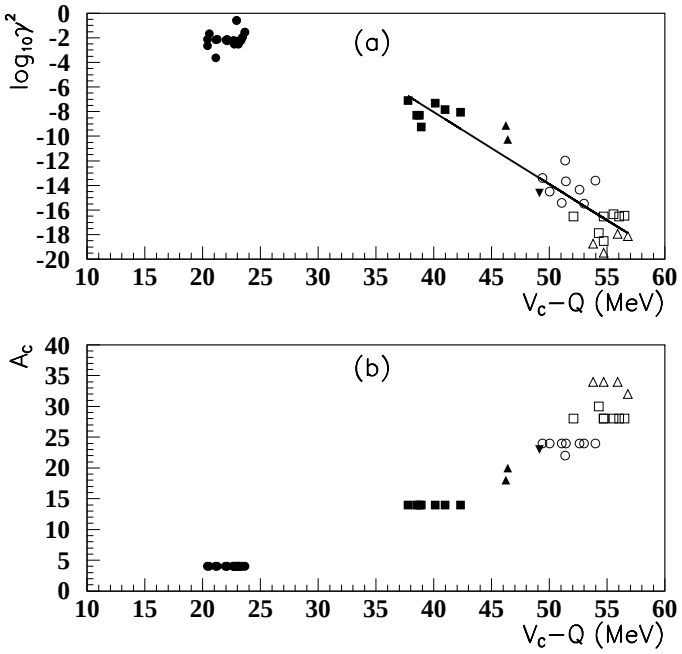

Fig. 2 – *(a)* The logarithm of the reduced width squared versus the fragmentation potential (6). Different symbols correspond to cluster decays in figure 2. The straight line is the linear fit (12) for cluster emission processes, except α-decay. *(b)* Cluster mass number versus the fragmentation potential.

in origin. Thus, the two different lines seen in proton emission systematics [14] can be directly connected with similar lines in figure 3 (b). They correspond to different orders of magnitude of the fragmentation potential, giving different orders to wave functions and therefore to reduced widths.

3. SHELL-MODEL DESCRIPTION OF DECAY PROCESSES

The amplitude to find an α-particle in a shell-model wave function of the parent nucleus is given by the following overlap

$$F(R_\alpha) = \langle \Psi_D \psi_\alpha | \Psi_P \rangle, \tag{14}$$

depending on the α-daughter distance R_α. Here, we denoted by $\Psi_{D/P}$ the many-body wave function of the daughter/parent nucleus built in terms of single particle orbitals generated by the nuclear mean field. On the other hand, ψ_α is the intrinsic wave function of the α-particle. Its radial part is a product of two-proton and two-neutron Gaussians, while the spin component is a singlet state [5]. By using as a residual interaction the pairing force, the formation amplitude becomes peaked on the nuclear surface.

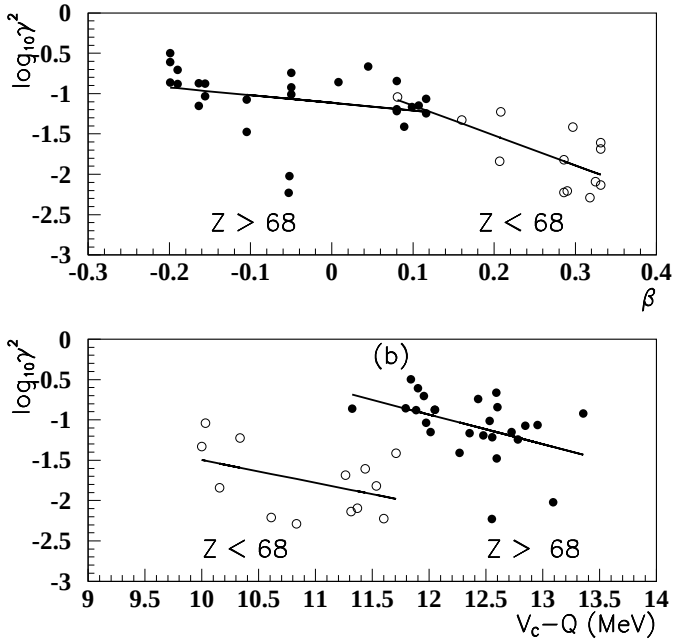

Fig. 3 – *(a)* The logarithm of the reduced width squared versus the quadrupole deformation. By open circles are given emitters with $Z < 68$, while by dark circles those with $Z > 68$ for proton emission. The two regression lines fit the corresponding data. *(b)* The logarithm of the reduced width squared versus the fragmentation potential (6). The symbols are the same as in *(a)*.

The binding energy per nucleon for an α-particle is much larger with respect to their neighbors. Due to a smaller nuclear density at surface, an α-cluster structure is energetically more favorable in this region. Therefore, clustering is a surface effect and in the previous Section we have shown that it can be simulated by assuming that the α-particle moves in a pocket-like potential centered at some radius R_0 on the nuclear surface.

Thus, in order to properly describe clustering properties at the single particle level one has to consider two components of the single particle orbitals, *i.e.*

$$\psi_l(r) = \mathcal{N}_l^{(SM)} \psi_l^{(SM)}(r) + \mathcal{N}_l^{(clus)} \psi_l^{(clus)}(r). \tag{15}$$

The shell model part has a standard spherical harmonic oscillator representation

$$\psi_l^{(SM)}(r) = \sum_n b_n \mathcal{R}_{nl}^{(\beta_0)}(r), \tag{16}$$

where $\beta_0 = M_N \omega/\hbar$ is the standard harmonic oscillator parameter and the principal quantum number has the values $N = 2n + l \leq 6$.

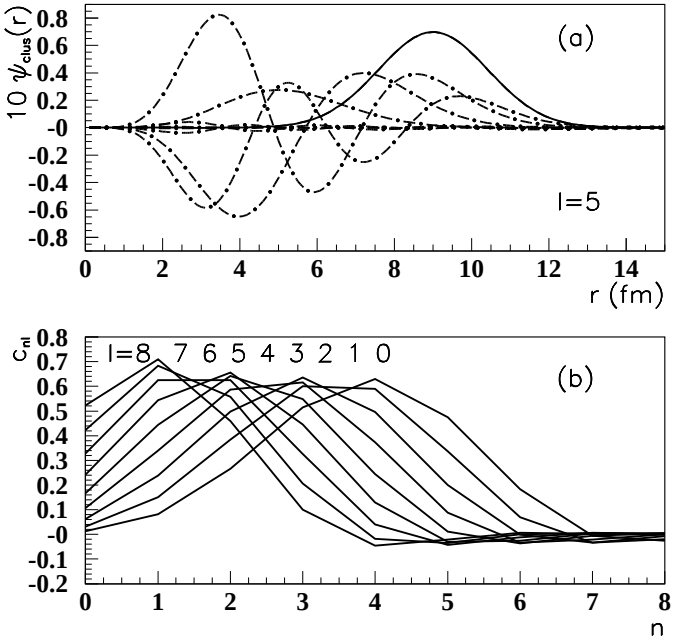

Fig. 4 – *(a)* Gaussian distribution centered on the nuclear surface (solid line) and various expansion terms (dot-dashed lines). *(b)* Expansion coefficients of a Gaussian centered on the nuclear surface given by (17).

For the cluster part one uses a wave function of the shifted oscillator

$$\psi_l^{(clus)}(r) = e^{-\beta_c(r-r_0)^2/2} = \sum_n c_n \mathcal{R}_{nl}^{(\beta)}(r) \,, \tag{17}$$

where N is spread around a larger value $N \sim 8-10$, as can be seen from figure 4. Notice that in [9] the harmonic oscillator parameter of the cluster part has a smaller value, *i.e.* $\beta < \beta_0$, in order to reduce the dimension of the single particle basis (15). Here all coefficients are found by a diagonalizing procedure of the Woods-Saxon mean field. *Actually, according to (5), the cluster parameter β should be proportional to the fragmentation potential, or to the Coulomb parameter χ in (6), in order to achieve a self consistent description of the emission process [16].*

The typical example of a heavy nucleus where the α-clustering effects are very important is ^{212}Po. Here, the structure of low-lying states can be explained in terms of two proton and two neutron orbitals above the double magic inert core ^{208}Pb [17]. Anyway, by using the standard components of the two protons and two neutrons the decay width is underestimated by two orders of magnitude. It is necessary to consider the second cluster component in (15), with $\mathcal{N}_l^{(clus)} = 0.3$, in order to describe the absolute value of the α-decay width, as can be seen in figure 5 (b) (solid line). In

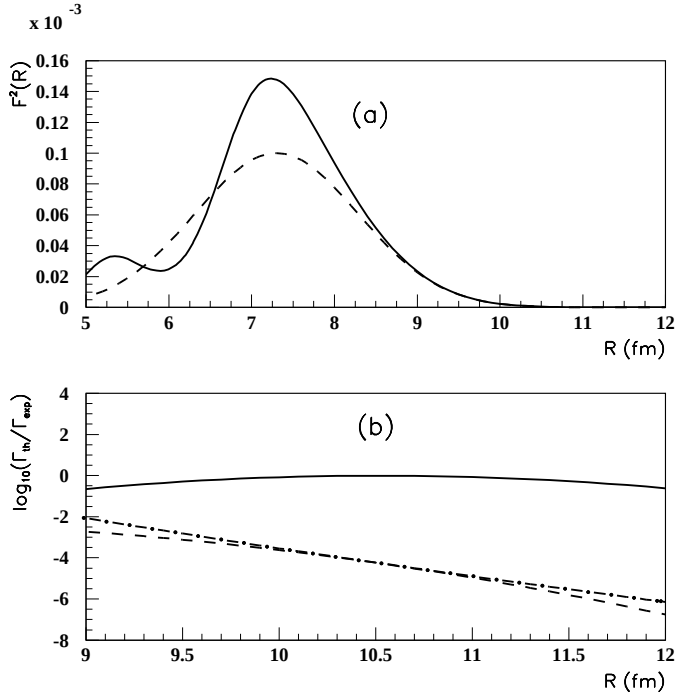

Fig. 5 – *(a)* α-particle formation probability for $^{212}Po \rightarrow ^{208}Pb + \alpha$. Dashed line: shell model, Solid line: shell model + α-cluster. *(b)* Logarithm of the ratio between the decay width and the experimental value as a function of the daughter-α-particle radius.

spite of the fact that in figure 5 (a) the difference between the formation probability within the shell model approach (dashed line) and mixed approach (solid line) is rather small, the enhancement of the decay width is about two orders of magnitude. Notice that the same value was obtained in [8], by using a diagonalizing procedure of the residual interaction.

This picture is also supported by analyzing electromagnetic transitions. The electric transition probability of the multipolarity λ is proportional to the reduced matrix element of the transition operator squared, *i.e.*

$$B(E\lambda : J \rightarrow J') = \frac{1}{2J+1} \left| \langle J' || \hat{T}_\lambda || J \rangle \right|^2, \tag{18}$$

where $|J\rangle$ and $|J'\rangle$ denote initial and final states and the transition operator is proportional to spherical harmonics

$$\hat{T}_{\lambda\mu} = r^\lambda Y_{\lambda\mu}. \tag{19}$$

The radial part of the quadrupole transition matrix element is proportional to the

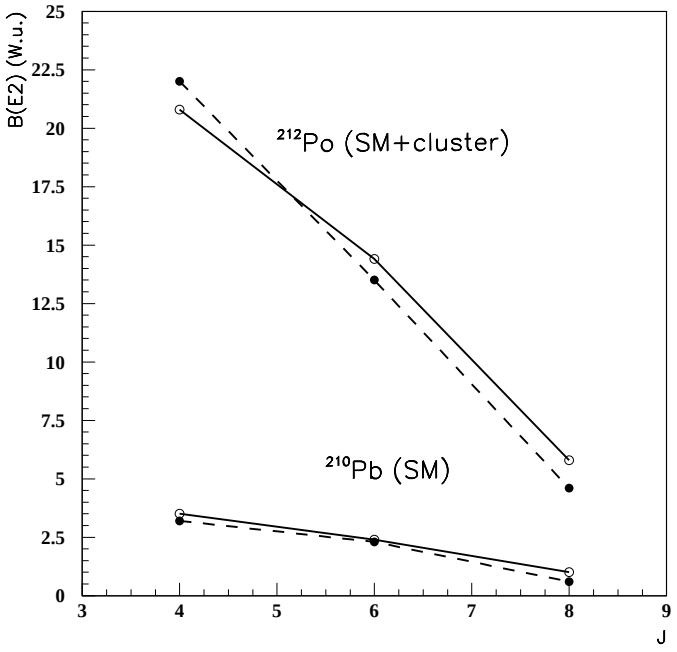

Fig. 6 – $B(E2: J \to J-2$ values (W.u.). Shell-model values in ^{210}Po and shell-model + cluster values in ^{212}Po (solid lines). By dashes are given experimental values.

principal quantum number

$$\langle n_1 l_1 | r^2 | n_2 l_2 \rangle \sim N = 2n + l. \tag{20}$$

As it is shown in figure 4, the clustering components are centered around the region $N \sim 8 - 10$ and therefore they should enhance transition probability.

It is known that B(E2) values are satisfactory described within the shell model for ^{210}Pb, but they are by one order of magnitude less than the experimental values in ^{212}Po. They are of the same order of magnitude as those in ^{210}Pb, given by the lower solid line in figure 6 [18]. In order to explain this discrepancy we used the mixed representation (15) with the same α-cluster amplitude. In figure 6 one indeed obtains a very good agreement of the computed values (upper solid line) with respect to experimental data (upper dashed line). This is a very convincing evidence in favor of the α-clustering structure of this nucleus.

4. CONCLUSIONS

Based on a simple model of the cluster-core dynamics, namely a shifted harmonic oscillator potential surrounded by the Coulomb interaction, it was derived an

universal analytical relation expressing the logarithm of the reduced width squared as a linear function in terms of the fragmentation potential, defined as the difference between the Coulomb barrier and the Q-value. It is fulfilled with a reasonable accuracy by all experimental decay data, describing transitions between ground states. In heavy nuclei this cluster component cannot be build from usual single particle orbitals because protons and neutron lie in different major shells. Thus, an additional Gaussian centered on the nuclear surface, predicted by the above mentioned universal law, is necessary to be included in the single particle basis. The ho parameter of the cluster part is proportional to the Coulomb parameter. We described both α-decay width and B(E2) value in ^{212}Po by using a mixed single particle basis, containing shell-model and α-cluster components.

Acknowledgments. This work was performed in the frame of the project PN-II-ID-PCE-2011-3-0092 of the Romanian Ministry of Education and Research.

REFERENCES

1. G. Gamow, Z. Phys. **51**, 204 (1928).
2. A. Săndulescu, R.Y. Cusson, W. Greiner, Lett. Nuovo Cim. **36**, 321 (1983).
3. B. Buck, A.C. Merchant, S.M. Perez, Phys. Rev. Lett. **72**, 1326 (1994).
4. S. Ohkubo, Phys. Rev. Lett. **74**, 2176 (1995).
5. H.J. Mang, Phys. Rev. **119**, 1069 (1960).
6. A. Săndulescu, Nucl. Phys. **37**, 332 (1962).
7. I. Tonozuka, A. Arima, Nucl. Phys. A **323**, 45 (1979).
8. K. Varga, R.G. Lovas, R.J. Liotta, Phys. Rev. Lett. **69**, 37 (1992).
9. D.S. Delion, A. Insolia, R.J. Liotta, Phys. Rev. C **54**, 292 (1996).
10. D.S. Delion, *Theory of particle and cluster emission* (Springer-Verlag, Berlin, 2010).
11. S. Peltonen, D.S. Delion, J. Suhonen, Phys. Rev. C **75**, 054301 (2007).
12. S. Peltonen, D.S. Delion, J. Suhonen, Phys. Rev. C **78**, 034608 (2008).
13. R. Blendowske, T. Fliessbach, H. Walliser, Z. Phys. A **339**, 121 (1991).
14. D.S. Delion, R.J. Liotta, R. Wyss, Phys. Rev. Lett. **96**, 072501 (2006).
15. E.L. Medeiros, M.M.N. Rodrigues, S.B. Duarte, O.A.P. Tavares, Eur. J. Phys. A **34**, 417 (2007).
16. D.S. Delion, A. Săndulescu, W. Greiner, Phys. Rev. C **69**, 044318 (2004).
17. D.S. Delion, J. Suhonen, Phys. Rev. C **61**, 024304 (2000).
18. A. Astier, P. Petkov, M.-G. Porquet, D.S. Delion, P. Schuck, Eur. Phys. J. A **47**, 165 (2010).